A light gradient boosting machine-based method for predicting the dynamic response of functionally graded plates

Do Thi Thanh Dieu*, Nguyen Hoang Yen

Faculty of Information Technology, Nguyen Tat Thanh University
*dttdieu@ntt.edu.vn

Abstract

The primary objective of this paper is to efficiently predict the dynamic response of functionally graded plates using LightGBM – a light gradient boosting machine, without reliance on supplementary analysis tools. To obtain the optimal LightGBM model, a dataset comprising 1,000 pairs of input and output is generated through iterations using a combination of isogeometric analysis (IGA) and third-order shear deformation plate theory (TSDT). In this model, the input is represented by a power index which governs the material distribution of the plate, and the output comprises 200 values illustrating deflection over time. To demonstrate the effectiveness of LightGBM in terms of accuracy and computational time, the results obtained by the proposed model are compared to those achieved with the optimal ANN, XGBoost models, and IGA.

Received 10/03/2024
Accepted 30/03/2024
Published 20/06/2024

Keywords

functionally graded plate, dynamic response, light gradient boosting machine, isogeometric analysis, artificial neural network, extreme gradient boosting

1 Introduction

Functionally Graded Material (FGM), a category of smart materials, is typically comprised of two main constituents: metal and ceramic. These materials exhibit various properties in different directions. The outstanding properties of FGMs result from the metal's remarkable fracture toughness and the ceramic's capacity to withstand high temperatures. FGMs are essential for resolving stress-related problems in laminated composite layers and successfully removing undesired stress discontinuities. Therefore, FGMs have found increasing use in a variety of industries, such as biology [1], aircraft engineering [2], and nuclear power plants [3].

Dynamic analysis issues related to functionally graded plates are currently garnering significant attention from researchers worldwide, owing to their remarkable features and diverse applications across various fields. For instance, the scaled boundary finite element method (SBFEM) was used to study the free vibration and transient dynamic behaviors of sandwich plates made of functionally graded material (FGM). The study demonstrates the method's efficiency in capturing free vibration and transient behaviors with high accuracy, reducing computational cost, and ensuring agreement with established solutions [4]. SBFEM has been extended to investigate the effects of fully coupled transient thermoelectricity in the modeling of fractures in functionally graded materials (FGMs) [5]. The nonlinear transient of porous FGM plates under step blast loading was analyzed using the finite element method. The obtained results were compared with benchmark solutions, and the effects of parameters such as power index, porosity parameter, and side-to-thickness ratio on the transient response of FGM plates subjected to step blast loads were examined [6]. Artificial neural networks (ANN) and

https://doi.org/10.55401/4x91s337

extreme gradient boosting (XGBoost) were utilized to rapidly predict the dynamic behavior of functionally graded plates [7]. Additionally, other investigations are documented in references [8, 9]. In the aforementioned studies, the traditional analytical methods were predominantly employed, leading to time-consuming and computationally expensive processes. Thus, this study introduces the light gradient boosting machine (LightGBM) as an efficient approach for dynamic analysis on functionally graded plates, aiming to reduce computational time without compromising accuracy.

Light gradient boosting machine (LightGBM) is a machine learning framework developed by Microsoft [10]. It belongs to the class of gradient boosting algorithms which are used for supervised learning tasks such as classification and regression. LightGBM is known for its speed, efficiency, and ability to handle large-scale datasets efficiently. As a result, LightGBM is applied in various fields [11-16]. For instance, LightGBM is used to predict the financing risk profile of 186 businesses to solve the persistent challenges of difficult and expensive financing for domestic and foreign enterprises [11]. In addition, LightGBM is used to identify the intrusive activities in the IoT network. The simulation results demonstrate that the proposed approach outperforms other evaluated methods, thus establishing its effectiveness and robustness for intrusion detection in an IoT environment [15]. LightGBM was combined with hyperparameter optimization algorithms such as Random, Grid, CMA-ES, and TPE to develop four hybrid models aimed at improving the accuracy of heating and cooling load predictions in residential buildings. Among these models, the TPE-LightGBM combination demonstrated the highest prediction accuracy [16]. Nevertheless, there has been no exploration in assessing the efficacy of LightGBM in forecasting the dynamic response of functionally graded plates.

To create a training dataset for LightGBM, isogeometric analysis (IGA) is proposed, utilizing non-uniform rational B-splines (NURBS) to represent both CAD geometry and FEA solution fields. IGA preserves exact geometry even at coarse discretization levels, effectively reducing degrees of freedom (DOFs) for high-order elements. Applied in diverse engineering fields, IGA has been demonstrated for analyzing functionally graded plates [17], efficient shell analysis of complex multi-patch structures [18], and others [19-23].

The precision of isogeometric analysis (IGA) has been verified through a comparison of results with existing literature [7]. In this study, IGA is employed to generate a dataset comprising 1,000 pairs, each of which consists of a power index controlling the plate's material distribution as input and output with 200 deflection values over time. This dataset is employed in training ANN, XGBoost, and LightGBM to determine optimal weights, thus enabling direct output prediction from input without additional analysis tools. Additionally, an exploration of parameter effects on accuracy and computational time is conducted to identify optimal models. The results of the LightGBM model are compared with those of IGA, ANN, and XGBoost to validate the effectiveness and robustness of LightGBM.

2 Methodology

2.1 Isogeometric analysis of functionally graded plates

2.1.1 Plate formulation

The displacement field of any point in the plate is described in this study using the third-order shear deformation plate theory (TSDT), as shown below [24]

$$\begin{Bmatrix} u_1 \\ u_2 \\ u_3 \end{Bmatrix} = \begin{Bmatrix} u \\ v \\ w \end{Bmatrix} + f(z) \begin{Bmatrix} \theta_x \\ \theta_y \\ 0 \end{Bmatrix} - g(z) \begin{Bmatrix} \dfrac{\partial w}{\partial x} \\ \dfrac{\partial w}{\partial y} \\ 0 \end{Bmatrix} \quad (1)$$

where θ_x and θ_y stand for the angular deformations; u, v and w indicate the spatial displacements. The descriptions of $f(z)$ and $g(z)$ are as follows.

$$f(z) = z - \frac{4z^3}{3h^2},\ g(z) = \frac{4z^3}{3h^2}, \quad (2)$$

The thickness of the plates is indicated by h, while the coordinate in the thickness direction is represented by z.

The strain-displacement relations can be explained as follows in accordance with the theory of infinitesimal elasticity:

$$\varepsilon_{xx} = \frac{\partial u}{\partial x} + f(z)\frac{\partial \theta_x}{\partial x} - g(z)\frac{\partial^2 w}{\partial x^2}, \quad (3)$$

$$\varepsilon_{yy} = \frac{\partial v}{\partial y} + f(z)\frac{\partial \theta_y}{\partial y} - g(z)\frac{\partial^2 w}{\partial y^2}, \quad (4)$$

$$\gamma_{xy} = \frac{\partial u}{\partial y} + \frac{\partial v}{\partial x} + f(z)\left(\frac{\partial \theta_x}{\partial y} + \frac{\partial \theta_y}{\partial x}\right) - g(z)\left(\frac{\partial^2 w}{\partial x \partial y} + \frac{\partial^2 w}{\partial x \partial y}\right), \quad (5)$$

$$\gamma_{xz} = f'(z)\theta_x + \left(1 - g'(z)\right)\frac{\partial w}{\partial x}, \quad (6)$$

$$\gamma_{yz} = f'(z)\theta_y + \left(1 - g'(z)\right)\frac{\partial w}{\partial y}. \quad (7)$$

The linear elastic constitutive equation is given by

$$\sigma_{xx} = Q_{11}\varepsilon_{xx} + Q_{12}\varepsilon_{yy}, \quad (8)$$

$$\sigma_{yy} = Q_{21}\varepsilon_{xx} + Q_{22}\varepsilon_{yy}, \quad (9)$$

$$\sigma_{xy} = Q_{44}\gamma_{xy};\ \sigma_{yz} = Q_{55}\gamma_{xy};\ \sigma_{xz} = Q_{66}\gamma_{xy}, \quad (10)$$

whereby

$$Q_{11} = Q_{22} = \frac{E}{1-\nu^2};\ Q_{12} = Q_{21} = \frac{E\nu}{1-\nu^2};\ Q_{44} = Q_{55} = Q_{66} = \frac{E}{2(1+\nu)}, \quad (11)$$

where $E = E(z)$ denotes the Poisson's ratio and $\nu = \nu(z)$ the Young's modulus, respectively. These variables, which are defined as follows, are considered to fluctuate along with the mass density (ρ) across the thickness of the plate in this study.

$$E(z) = E_c V_c + E_m V_m, \quad (12)$$

$$\nu(z) = \nu_c V_c + \nu_m V_m, \quad (13)$$

$$\rho(z) = \rho_c V_c + \rho_m V_m, \quad (14)$$

where $V_c + V_m = 1$ and c and m stand for the constituents of ceramic and metal, respectively; $V_c(z)$ and $V_m(z)$ are the volume fractions of ceramic and metal, respectively.

The equation of motion for the following problem can be stated as follows by using Hamilton's principle [25]:

$$\int_{-h/2}^{h/2} \left(\delta T - \delta U - \delta W_e\right) dt = 0, \quad (15)$$

where W_e stands for the work performed by outside forces, U for elastic energy, and T for kinetic energy. These terms' variational form formulations are given by

$$\delta T = \int_V \rho \dot{u}_i \delta \dot{u}_i dV, \quad (16)$$

$$\delta U = \int_V \sigma_{ij} \delta \varepsilon_{ij} dV, \quad (17)$$

$$\delta W_e = -\int_\Gamma \hat{t}_i \delta u_i d\Gamma, \quad (18)$$

When $\hat{t}_i$ indicates the external loads operating on area Γ, V is the plate's volume, and the dot superscript stands for the derivative with regard to time t.

Equations (3)-(7) and (16)-(18) can be used in place of (15) to rewrite the equation of motion, along with a few other modifications:

$$\int_\Omega \delta \hat{\boldsymbol{\varepsilon}}^T \hat{\mathbf{D}} \hat{\boldsymbol{\varepsilon}} d\Omega + \int_\Omega \delta \bar{\mathbf{u}}^T \mathbf{m} \ddot{\bar{\mathbf{u}}} d\Omega = \int_\Omega q(t) \delta w d\Omega, \quad (19)$$

where Ω stands for the plate's reference plane and $q(t)$, which is the distributed load applied to the plate's upper surface, is dependent on the time t variable. For detailed information regarding the quantities specified in the preceding equation, we refer readers to [26].

2.1.2 Isogeometric analysis

The IGA approach is used in this study to model the plate [27]. The NURBS basis function $R_{i,j}^{p,q}(\xi,\eta)$ is used to discretize the equation of motion. The eth NURBS element's displacement, u, is provided by

$$\mathbf{u} = \sum_{i=1}^{ncp} R_i(\xi,\eta)\mathbf{d}_i, \quad (20)$$

where the variables for displacement associated with the *ith* control point are denoted by $\mathbf{d}_i = \{u_i \quad v_i \quad \theta_{xi} \quad \theta_{yi} \quad w_i\}^T$, and $\mathbf{u} = \{u \quad v \quad \theta_x \quad \theta_y \quad w\}^T$ represents the displacement vector.

Equation (19) can be substituted with equation (20), resulting in the following new equation for the system:

$$\mathbf{M}\ddot{\mathbf{d}} + \mathbf{K}\mathbf{d} = \mathbf{q}(t), \quad (21)$$

where $q(t)$ denotes the load vector and **M** and **K** stand for the mass and stiffness matrices, respectively. The readers may find further details in [26].

In this analysis, only structural damping of the plate is considered. The Rayleigh damping method is used to simulate the damping, and the proportional damping matrix is defined by

$$\mathbf{C} = a_0\mathbf{M} + a_1\mathbf{K}, \quad (22)$$

in which

$$a_1 = \frac{2\zeta}{\omega_1 + \omega_2}, \quad a_0 = \omega_1 \omega_2 a_1, \qquad (23)$$

where ω_1 and ω_2 are the natural frequencies of the first and second vibration modes, respectively, and ζ is the damping ratio of the first and second vibration modes [28].

The system's equation in (21) with the damping matrix included is rewritten as follows:

$$\mathbf{M}\ddot{\mathbf{d}} + \mathbf{C}\dot{\mathbf{d}} + \mathbf{K}\mathbf{d} = \mathbf{q}(t). \qquad (24)$$

The Newmark technique is applied to solve the time-dependent problem as given in (24) [29]. The overall process for resolving the temporary issue is provided in [26].

2.2 The light gradient boosting machine model

The LightGBM algorithm, which is a relatively recent algorithm, is explained in length in this section. LightGBM and a unique GBDT (Gradient Boosting Decision Tree) algorithm have been used in a wide range of data mining applications, including ordering, regression, and classification [10]. Two innovative methods are included in the LightGBM algorithm: exclusive feature bundling and gradient-based one-side sampling, respectively.

Considering the supervised training set $X = \{(x_i, y_i)\}_{i=1}^{n}$, LightGBM seeks to minimize the expected value of a particular loss function $L(y, f(x))$ by determining an approximation $\hat{f}(x)$ to a particular function $f^*(x)$ as follows:

$$\hat{f} = \arg\min_{f} E_{y,X} L(y, f(x)) \qquad (25)$$

The final model is approximated by LightGBM by integrating multiple T regression trees $\sum_{t=1}^{T} f_t(x)$.

$$f_T(X) = \sum_{t=1}^{T} f_t(x) \qquad (26)$$

The expression $w_q(x)$, $q \in \{1, 2, \ldots, J\}$ represents the regression trees, where J represents the number of leaves, q represents the tree's decision rules, and w is a vector representing the sample weight of leaf nodes. Thus, at step t, LightGBM would receive the following additive training:

$$\Gamma_t = \sum_{i=1}^{n} L(y_i, F_{t-1}(x_i) + f_t(x_i)) \qquad (27)$$

Newton's approach is used in LightGBM to quickly approximate the goal function. The following transformation can be applied to the formulation after the constant term in (27) is removed for simplicity:

$$\Gamma_t \cong \sum_{i=1}^{n} \left(g_i f_t(x_i) + \frac{1}{2} h_i f_t^2(x_i) \right) \qquad (28)$$

where the loss function's first- and second-order gradient statistics are represented by the symbols g_i and h_i. (28) could be changed as follows, where I_j represents the sample set of leaf j.

$$\Gamma_t \cong \sum_{j=1}^{j} \left(\left(\sum_{i \in I_j} g_i \right) w_j + \frac{1}{2} \left(\left(\sum_{i \in I_j} h_i + \lambda \right) w_j^2 \right) \right) \qquad (29)$$

The ideal leaf weight scores of every leaf node w_j^* and the extreme value of Γ_K for a given tree structure $q(x)$ could be determined in the manner described below:

$$w_j^* = -\frac{\sum_{i \in I_j} g_i}{\sum_{i \in I_j} h_i + \lambda} \qquad (30)$$

$$\Gamma_T^* = -\frac{1}{2} \sum_{j=1}^{J} \frac{\left(\sum_{i \in I_j} g_i \right)^2}{\sum_{i \in I_j} h_i + \lambda} \qquad (31)$$

where the quality of the tree structure q is measured by a scoring function denoted as Γ_T^*. Lastly, following the split addition, the objective function is:

$$G = \frac{1}{2} \left(\frac{\left(\sum_{i \in I_L} g_i \right)^2}{\sum_{i \in I_L} h_i + \lambda} + \frac{\left(\sum_{i \in I_R} g_i \right)^2}{\sum_{i \in I_R} h_i + \lambda} - \frac{\left(\sum_{i \in I} g_i \right)^2}{\sum_{i \in I} h_i + \lambda} \right) \qquad (32)$$

where the left and right branches' respective sample sets are denoted by I_L and I_R. LightGBM is an excellent way to process large-scale data and features because while typical GBDT-based techniques like XGBoost and GBDT grow trees horizontally, LightGBM would develop the tree vertically.

In general, the hyper-parameters would have a big impact on forecasting accuracy. Therefore, we need to ascertain the number and the range of variation of LightGBM's hyper-parameter before utilizing it. Table 1 displays the key LightGBM parameters.

Table 1 The primary LightGBM model hyperparameters adjusted in this investigation

Hyperparameters	Explanation and application	Default
learning_rate	Regulate the pace of shrinking; A smaller value corresponds to a shorter iteration step.	0.1
Max_depth	Limit a tree model's maximum depth	case-based
num_interations	The quantity of trees (iterations)	100
num_leaves	Limit the decision tree's maximum number of leaves.	31
num_bin	Regulate the maximum number of bins (data intervals) when converting the input layer parameter dataset into a histogram.	255
n_estimators	Number of trees. Underfitting will result from n_estimators being too small.	100

3 Results and discussions

In the previous study by the author, the accuracy of dynamic analysis of isotropic square plates using IGA and TSDT was verified [7]. In the present study, LightGBM has been utilized instead of IGA to examine dynamic response of the Al_2O_3/Al square plate (as shown in Figure 1) with $h=a/20$ and the damping ratio ζ of 0.05 quickly. The results obtained from the present method will be contrasted with those of the optimal ANN and XGBoost models. Material properties of Al_2O_3/Al plate are given as follows:

ceramic Al_2O_3 : $E_c=380GPa, v_c=0.3, \rho_c=3800\,\mathrm{kg/m^3}$

metal Al: $E_m=70GPa, v_m=0.3, \rho_m=2707\,\mathrm{kg/m^3}$

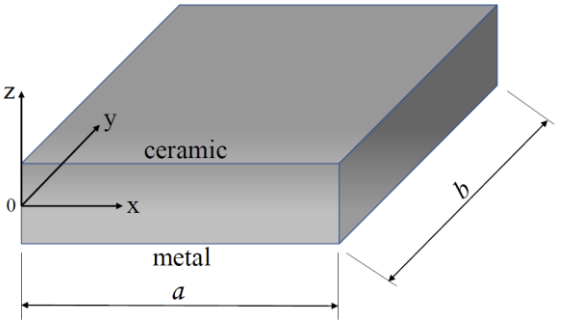

Figure 1 The functionally graded plate model

The following function governs the distribution of the ceramic composition in the Al_2O_3/Al plate along the thickness of the plate:

$$V_c=\left(\frac{z}{h}+\frac{1}{2}\right)^{n_z} \tag{33}$$

where V_c stands for the ceramic volume fraction, n_z indicates the power index on the z-axis, and h represents the plate thickness.

A sudden uniformly distributed dynamic load with $q_0=-0.5\times10^8\,\mathrm{N/m^2}$ is applied to the plate under the CCCC boundary condition, which is depicted as follows:

$$u=v=\theta_x=\theta_y=w=\frac{\partial w}{\partial n}=0 \text{ at all edges} \tag{34}$$

IGA generated 1000 data pairs, which were used to execute the training process in ANN, XGBoost, and LightGBM to obtain optimal weights in models. Specifically, n_z is regarded as an input with values between 0 and 10, and the output consists of 200 deflections versus time values that can be explained as follows:

$$\bar{t}=t\sqrt{\frac{E_m}{a^2\rho_m}};\ \bar{w}=\frac{10^3 D_0}{q_0 a^4}w;\ D_0=\frac{E_c h_0^3}{12\left(1-v_c^2\right)} \tag{35}$$

These 1,000 data pairs are splitted into two groups: the first group contains 900 pairs that are used in the training phase, and the other contains 100 pairs that are used in the testing phase. Optimal models for ANN and XGBoost were determined after investigating the influence of various parameters on model accuracy and computational time presented in the authors' preceding study [7]. The aim of this study is to select the optimal LightGBM model by examining the impact of

parameters such as the number of trees (n_estimators), maximum tree depth (max_depth), and learning rate (learning_rate) on the effectiveness of LightGBM. Subsequently, a comparation is conducted to assess the accuracy and computational efficiency of the optimal ANN, XGBoost, and LightGBM models.

The training process is conducted through Python 3.7 on a laptop featuring an Intel® CoreTM i7-8550U CPU @ 1.80 GHz 2.00 GHz, 12.0 GB RAM, and operating on Windows 11 with a 64-bit system.

The performance of the ANN, XGBoost, and LightGBM models was assessed in terms of mean square error (MSE), mean absolute percentage error (MAPE), and computational time. In the LightGBM model, the parameter of the number of trees (n_estimators) with values selected in the set {10, 30, 50, 100, 150, 200, 500 and 1,000} is investigated first. The remaining parameters are set to default as in the system. The gained results are shown in Table 2.

Table 2 The effect of the number of trees on the effectiveness of the training and testing processes in LightGBM

n_estimators		10	30	50	**100**	150	200	500	1,000
MSE	Training	2.21E-04	4.49E-06	1.19E-06	**1.11E-06**	1.10E-06	1.10E-06	1.09E-06	1.09E-06
	Testing	2.27E-04	3.64E-06	5.30E-07	**4.78E-07**	4.70E-07	4.67E-07	4.64E-07	4.66E-07
MAPE	Training	2.0158	0.2543	0.0684	**0.0551**	0.0547	0.0544	0.0540	0.0540
	Testing	2.0269	0.2489	0.0688	**0.0541**	0.0536	0.0533	0.0529	0.0529
Time (second)		2.0269	3.5708	4.5090	**7.7034**	11.0322	15.5520	46.8837	99.3168

As can be seen from the table, LightGBM with n_estimators of 100 produces a trade-off between computational time and accuracy. Specifically, it takes 7.7 seconds, and with an accuracy rate of 99.9449 % for training and 99.9459 % for testing. Therefore, the model with n_estimators of 100 is utilized in the next investigation. Subsequently, the max depth of the trees (max_depth) is examined and gained results are indicated in Table 3.

Table 3 The effect of the max depth of the trees on the effectiveness of the training and testing processes in LightGBM

max_depth		**1**	**2**	**3**	**5**	**7**	**10**
MSE	Training	8.33E-06	1.43E-06	1.16E-06	**1.11E-06**	1.11E-06	1.11E+00
	Testing	7.95E-06	8.47E-07	5.47E-07	**4.82E-07**	4.79E-07	4.78E-07
MAPE	Training	0.2764	0.1008	0.0719	**0.0566**	0.0552	0.0551
	Testing	0.2731	0.1007	0.0703	**0.0552**	0.0542	0.0541
Time (second)		2.3131	2.5471	3.3438	**5.5624**	7.2807	7.7408

The table shows that when the tree reaches a depth of 5, the model accuracy stabilizes, and computational time increases as the max depth of the tree increases. As a result, the LightGBM model with n_estimators of 100 and max_depth of 5 is used for determining the learning rate. Table 4 shows the effect of the learning rate on the accuracy and computational time of the LightGBM model.

Table 4 The effect of the learning rate on the effectiveness of the training and testing processes in LightGBM

learning_rate		0.01	0.05	**0.1**	0.3	0.5	0.7	1
MSE	Training	2.44E-04	1.20E-06	**1.11E-06**	1.14E-06	1.17E-06	1.14E-06	1.11E-06
	Testing	2.50E-04	5.41E-07	**4.82E-07**	5.08E-07	5.54E-07	5.21E-07	4.83E-07
MAPE	Training	2.1184	0.0719	**0.0566**	0.0686	0.0747	0.0691	0.060743
	Testing	2.1303	0.0723	**0.0552**	0.0673	0.0744	0.0685	0.059671
Time (second)		6.3431	6.5397	**5.7967**	4.4376	3.9618	4.3115	5.71561

Table 4 demonstrates that the LightGBM model, with a learning rate of 0.1 yields optimal results, achieving 5.7967 seconds for training with an accuracy of 99.9434 %, and 99.9448 % for testing. Consequently, the LightGBM model with 100 trees, a maximum depth tree of 5, and a learning rate of 0.1 is the most effective model in this study for predicting the dynamic response of FG plates. Figure 2 displays the results that this model accurately predicted, with a rate of over 99.9 % in comparison with results obtained by IGA.

The parameters in the two models, ANN and XGBoost, were also examined in previous studies [7] to determine which model architecture was most effective in predicting the dynamic response of FG plates. Two optimal models were identified: XGBoost with max_depth of 5, n_estimators of 200, and a learning rate of 0.1; and the ANN model with Adam optimizer, ReLU function, 3,000 epochs, two hidden layers, and 50 nodes at each. Results obtained by the LightGBM are compared to those of the optimal ANN and XGBoost models in Table 5.

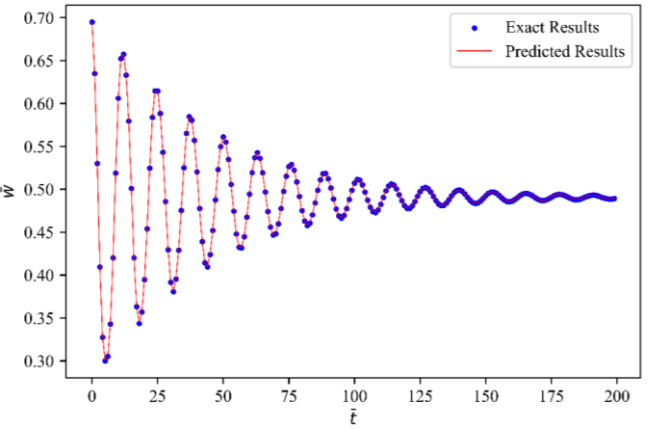

Figure 2 Dynamic response of the Al2O3/Al plate predicted by using LightGBM

Table 5 A comparison between ANN, XGBoost, and LightGBM in terms of the accuracy and computational time

Model		**ANN**	**XGBoost**	**LightGBM**
MSE	Training	1.63E-05	8.89E-08	1.11E-06
	Testing	1.48E-05	2.57E-07	4.82E-07
MAPE	Training	0.3724	0.0294	0.0566
	Testing	0.5977	0.0526	0.0552
Time (second)		46.1856	15.6894	5.7967

As indicated in the table, the MAPE values for both the training and testing datasets obtained with LightGBM are nearly identical. Furthermore, LightGBM not only ensures accurate prediction of dynamic responses for the FG plate but also significantly reduces computational time compared to ANN and XGBoost.

4 Conclusion and future research

This paper successfully introduces the development of LightGBM for modeling the dynamic response of functionally graded plates with various material properties, along the thickness. The study employs a dataset with the power index as the single input, and 200 output values representing deflection over time. Utilizing this dataset, this study identifies the optimum LightGBM architecture for plate behavior prediction without requiring additional analytical tools. Additionally, an investigation has been conducted into the impact of parameters on model accuracy and computational time to identify the most effective configurations. The accuracy of the LightGBM model is verified through a comparison of its results with those derived from IGA. From the obtained results, it is evident that LightGBM not only achieves over 99.9 % of accuracy but also significantly reduces computational time compared to ANN and XGBoost. The current methodology holds the potentials for application to more intricate engineering challenges, such as multi-directional functionally graded plates or shells. Furthermore, optimization aspects merit further investigation.

References

1. Talukdar, R. G., Saviour, C. M., Dhara, S., & Gupta, S. (2023). Biomechanical analysis of functionally graded porous interbody cage for lumbar spinal fusion. *Computers in Biology and Medicine*, 164, 107281. https://doi.org/10.1016/j.compbiomed.2023.107281
2. Chen, D., Gao, K., Yang, J., & Zhang, L. (2023). Functionally graded porous structures: Analyses, performances, and applications – A Review. *Thin-Walled Structures*, 191, 111046. https://doi.org/10.1016/j.tws.2023.111046
3. Klecka, J., Cizek, J., Matejicek, J., Lukac, F., & Vala, J. (2023). Thick functionally-graded W-316L composite coatings for nuclear fusion applications. *Nuclear Materials and Energy*, 34, 101373. https://doi.org/10.1016/j.nme.2023.101373
4. Liu, J., Hao, C., Ye, W., Yang, F., & Lin, G. (2021). Free vibration and transient dynamic response of functionally graded sandwich plates with power-law nonhomogeneity by the scaled boundary finite element method. *Computer Methods in Applied Mechanics and Engineering*, 376, 113665. https://doi.org/10.1016/j.cma.2021.113665
5. Iqbal, M. D., Birk, C., Ooi, E. T., Natarajan, S., & Gravenkamp, H. (2023). Transient thermoelastic fracture analysis of functionally graded materials using the scaled boundary finite element method. *Theoretical and Applied Fracture Mechanics*, 127, 104056. https://doi.org/10.1016/j.tafmec.2023.104056
6. Karakoti, A., Pandey, S., & Kar, V. R. (2021). Nonlinear transient analysis of porous functionally graded material plates under blast loading. *Materials Today: Proceedings*, 46, 8111–8113. https://doi.org/10.1016/j.matpr.2021.03.051
7. Do, D. T. T., & Thai, S. (2023). Transient analysis of functionally graded plates using extreme gradient boosting. *Journal of Science and Technology in Civil Engineering (JSTCE) − HUCE*, 17(4), Article 4. https://doi.org/10.31814/stce.huce2023-17(4)-03
8. Karamanli, A., Vo, T. P., & Civalek, O. (2023). Higher order finite element models for transient analysis of strain gradient functionally graded microplates. *European Journal of Mechanics − A/Solids*, 99, 104933. https://doi.org/10.1016/j.euromechsol.2023.104933
9. Avramov, K., Uspensky, B., Sakhno, N., & Nikonov, O. (2022). Transient response of functionally graded carbon nanotubes reinforced composite conical shell with ring-stiffener under the action of impact loads. *European Journal of Mechanics − A/Solids*, 91, 104429. https://doi.org/10.1016/j.euromechsol.2021.104429
10. Ke, G., Meng, Q., Finley, T., Wang, T., Chen, W., Ma, W., Ye, Q., & Liu, T.-Y. (2017). LightGBM: A Highly Efficient Gradient Boosting Decision Tree. *Advances in Neural Information Processing Systems*, 30. https://proceedings.neurips.cc/paper_files/paper/2017/hash/6449f44a102fde848669bdd9eb6b76fa-Abstract.html
11. Wang, D., Li, L., & Zhao, D. (2022). Corporate finance risk prediction based on LightGBM. *Information Sciences*, 602, 259-268. https://doi.org/10.1016/j.ins.2022.04.058
12. Li, Z., Xu, W., & Li, A. (2022). Research on multi factor stock selection model based on LightGBM and Bayesian Optimization. *Procedia Computer Science*, 214, 1234-1240. https://doi.org/10.1016/j.procs.2022.11.301
13. Deng, S., Su, J., Zhu, Y., Yu, Y., & Xiao, C. (2024). Forecasting carbon price trends based on an interpretable light gradient boosting machine and Bayesian optimization. *Expert Systems with Applications*, 242, 122502. https://doi.org/10.1016/j.eswa.2023.122502
14. Omotehinwa, T. O., Oyewola, D. O., & Dada, E. G. (2023). A Light Gradient-Boosting Machine algorithm with Tree-Structured Parzen Estimator for breast cancer diagnosis. *Healthcare Analytics*, 4, 100218. https://doi.org/10.1016/j.health.2023.100218
15. Mishra, D., Naik, B., Nayak, J., Souri, A., Dash, P. B., & Vimal, S. (2023). Light gradient boosting machine with optimized hyperparameters for identification of malicious access in IoT network. *Digital Communications and Networks*, 9(1), 125–137. https://doi.org/10.1016/j.dcan.2022.10.004
16. Guo, J., Yun, S., Meng, Y., He, N., Ye, D., Zhao, Z., Jia, L., & Yang, L. (2023). Prediction of heating and cooling loads based on light gradient boosting machine algorithms. *Building and Environment*, 236, 110252. https://doi.org/10.1016/j.buildenv.2023.110252

17. Son, T., & Qui, L. X. (2022). Investigate the bending and free vibration responses of multi-directional functionally graded plates with variable thickness based on isogeometric analysis. *Journal of Science and Technology in Civil Engineering (JSTCE) − HUCE*, 16(4), Article 4.
18. Farahat, A., Verhelst, H. M., Kiendl, J., & Kapl, M. (2023). Isogeometric analysis for multi-patch structured Kirchhoff-Love shells. *Computer Methods in Applied Mechanics and Engineering*, 411, 116060. https://doi.org/10.1016/j.cma.2023.116060
19. Do, D. T. T., Nguyen, A. T., & Nguyen, N. V. (2023). An isogeometric approach of static, free vibration and buckling analyses of multilayered solar cell structures. *International Journal of Mechanics and Materials in Design*. https://doi.org/10.1007/s10999-023-09686-1
20. Do, Dieu. T. T., Lee, D., & Lee, J. (2019). Material optimization of functionally graded plates using deep neural network and modified symbiotic organisms search for eigenvalue problems. *Composites Part B: Engineering*, 159, 300-326. https://doi.org/10.1016/j.compositesb.2018.09.087
21. Wang, S., Hong, J., Yin, S., & Zhang, G. (2024). Isogeometric analysis of magneto-electro-elastic functionally graded Mindlin microplates. *Thin-Walled Structures*, 111740. https://doi.org/10.1016/j.tws.2024.111740
22. Thai, S., Do, D. T. T., & Tan, T. N. (2023). Nonlinear bending analysis of variable thickness multi-directional functionally graded plates based on isogeometric analysis. *Mechanics of Advanced Materials and Structures*, 30(20), 4091–4109. https://doi.org/10.1080/15376494.2022.2088909
23. Verhelst, H. M., Weinmüller, P., Mantzaflaris, A., Takacs, T., & Toshniwal, D. (2024). A comparison of smooth basis constructions for isogeometric analysis. *Computer Methods in Applied Mechanics and Engineering*, 419, 116659. https://doi.org/10.1016/j.cma.2023.116659
24. A Simple Higher-Order Theory for Laminated Composite Plates | Semantic Scholar. (n.d.). Retrieved March 8, 2024, from https://www.semanticscholar.org/paper/A-Simple-Higher-Order-Theory-for-Laminated-Plates-Reddy/7a74d17c58e68222dc951e9307f80e58bb985828
25. Hamilton, W. R. (1834). On a General Method in Dynamics; By Which the Study of the Motions of All Free Systems of Attracting or Repelling Points is Reduced to the Search and Differentiation of One Central Relation, or Characteristic Function. *Philosophical Transactions of the Royal Society of London*, 124, 247-308.
26. Tran, M. T., & Thai, S. (2023). Transient analysis of variable thickness multi-directional functionally graded plates using isogeometric analysis. *Multidiscipline Modeling in Materials and Structures*, 19(4), 652-679. https://doi.org/10.1108/MMMS-12-2022-0283
27. Hughes, T. J. R., Cottrell, J. A., & Bazilevs, Y. (2005). Isogeometric analysis: CAD, finite elements, NURBS, exact geometry and mesh refinement. *Computer Methods in Applied Mechanics and Engineering*, 194(39), 4135-4195. https://doi.org/10.1016/j.cma.2004.10.008
28. Kareem, A., & Gurley, K. (1996). Damping in structures: Its evaluation and treatment of uncertainty. *Journal of Wind Engineering and Industrial Aerodynamics*, 59(2), 131-157. https://doi.org/10.1016/0167-6105(96)00004-9
29. Newmark, N. M. (1959). A Method of Computation for Structural Dynamics. *Journal of the Engineering Mechanics Division*, 85(3), 67-94. https://doi.org/10.1061/JMCEA3.0000098

Phương pháp dựa trên thuật toán tăng cường độ dốc nhẹ cho dự đoán đáp ứng động lực học của tấm cơ tính biến thiên

Đỗ Thị Thanh Diệu*, Nguyễn Hoàng Yến
Khoa Công nghệ Thông tin, Trường Đại học Nguyễn Tất Thành
dttdieu@ntt.edu.vn

Tóm tắt Mục tiêu chính của bài viết này là để dự đoán một cách hiệu quả đáp ứng động lực học của các tấm cơ tính biến thiên bằng cách sử dụng thuật toán tăng cường độ dốc nhẹ (LightGBM) mà không phụ thuộc vào bất kỳ công cụ phân tích nào. Để thu được mô hình LightGBM tối ưu, một tập dữ liệu bao gồm 1 000 cặp dữ liệu đầu vào và đầu ra được tạo ra thông qua các lần lặp bằng cách sử dụng kết hợp phân tích đẳng hình học (IGA) và lý thuyết tấm biến dạng cắt bậc ba (TSDT). Trong mô hình này, đầu vào là chỉ số mũ, nó chi phối sự phân bố vật liệu của tấm, và đầu ra bao gồm 200 giá trị minh họa chuyển vị theo thời gian. Để chứng minh tính hiệu quả của mô hình LightGBM về độ chính xác và thời gian tính toán, kết quả thu được từ mô hình đề xuất được so sánh với các kết quả đạt được bởi các mô hình tối ưu ANN, XGBoost và IGA.

Từ khóa tấm cơ tính biến thiên; đáp ứng động lực học; thuật toán tăng cường độ dốc nhẹ; phân tích đẳng hình học; mạng thần kinh nhân tạo; thuật toán tăng cường độ dốc cực cao.